Nanowire antenna emission

Grzegorz Grzela,[*,†] Ramón Paniagua-Domínguez,[‡] Tommy Barten,[†] Yannik Fontana,[†,§] José A. Sánchez-Gil,[‡] and Jaime Gómez Rivas[†,¶]

FOM Institute for Atomic and Molecular Physics (AMOLF), c/o Philips Research, High-Tech Campus 4, 5656 AE Eindhoven, The Netherlands, Instituto de Estructura de la Materia (IEM-CSIC), Consejo Superior de Investigaciones Científicas, Serrano 121, E-28006 Madrid, Spain, and COBRA Research Institute, Eindhoven University of Technology, P.O. Box 513, 5600 MB Eindhoven, The Netherlands

E-mail: grzela@amolf.nl

Abstract

We experimentally demonstrate the directional emission of polarized light from single semiconductor nanowires. The directionality of this emission has been directly determined with Fourier micro-photoluminescence measurements of vertically oriented InP nanowires. Nanowires behave as efficient optical nanoantennas, with emission characteristics that are not only given by the material but also by their geometry and dimensions. By means of finite element simulations, we show that the radiated power can be enhanced for frequencies and diameters at which leaky modes in the structure are present. These leaky modes can be associated to Mie resonances in the cylindrical structure. The radiated power can be also inhibited at other frequencies or when the coupling of the emission to the resonances is not favored. We

[*]To whom correspondence should be addressed
[†]FOM Institute for Atomic and Molecular Physics (AMOLF)
[‡]Consejo Superior de Investigaciones Científicas (CSIC)
[¶]Eindhoven University of Technology (TU/e)
[§]Current address: Laboratoire des Matériaux Semiconducteurs, Institut des Matériaux, Ecole Polytechnique Fédérale de Lausanne, 1015 Lausanne, Switzerland

anticipate the relevance of these results for the development of nanowire photon sources with optimized efficiency and/or controlled emission by the geometry.

Keywords: semiconductor nanowires, nanoantennas, directional emission, Fourier microscopy

The directionality of the light emission plays a key role in the design of efficient sources. The control of this property will improve the performance of devices such as light emitting diodes, nano-lasers or single photon sources. In this regard, the recent progress in nano-fabrication techniques has led to an increased interest in the optical properties of novel structures. Among those nanostructures, semiconductor nanowires have shown vast possibilities to enhance light absorption and to control the polarization and the wavelength of the light emission. The bottom-up fabrication process has enabled the growth of semiconductor nanowires on top of various materials despite of a mismatch in the crystal lattice parameter .[1,2] This property brought interesting heterostructures to life, such as superlattices,[3] radially stacked quantum wells,[4] individual or nanowire photonic crystal lasers[5–7] or single photon emitters embedded in nanowires.[8–10] Due to their geometry, nanowires show anisotropic optical properties. The evidence of such behavior was found in the polarization dependent absorption cross section and the light emission from nanowires.[11] Those phenomena have been described in the context guided modes in finite nanowires,[12] and Mie resonances in infinitely long cylinders.[9,13,14] The same properties enable the increase of the absorption by nanowires and their potential use as solar light absorbers in photovoltaic applications.[15,16] This resonant response in the absorption of nanowires has been ascribed to a nanoantenna-like response in the nanostructures. However, an antenna behavior implies not only a resonant behavior but also a directional response. Due to their finite length, semiconductor nanowires can form cavities in which guided modes can lead to lasing.[17] By analyzing the interference pattern of the emission from the end-facets of nanowires, the highly diffractive emission from the subwavelength facets was established.[18] Waveguide modes are also responsible for shaping the emission from luminescent nitrogen-vacancy centers in diamond nanowires.[19] Although the directionality of the emission from nanowires has been theoretically studied,[20,21] no measurements have been reported so far.

In this manuscript, we present the first demonstration of the directional photoluminescence emission from vertical nanowires. The measurements have been done on individual InP nanowires using Fourier microscopy. Semiconductor nanowires behave as true nanoantennas with a direc-

tional emission of polarized light. As in RF antennas, the directionality is determined by the geometry and dimensions of the radiating structure.[22,23] Simulations of the emission of an oriented dipole in the nanowires reveal its coupling to leaky modes, giving rise to the directional far-field emission pattern. We also show that a dipole oriented perpendicular to the axis of the nanowire produces a qualitatively and quantitatively different emission pattern than the one produced by a dipole oriented parallel to the axis. Besides of the directionality, the nanowire modifies the local density of optical states (LDOS) to which the radiating dipole can decay. This leads to an increased emission efficiency of a dipole oriented parallel to the axis of the nanowire compared to the emission of a dipole in free space. These results are of relevance for the design of single photon sources where a controlled directionality and polarization of the emission will play a key role in their integration in optoelectronic circuits.

Nanowire description. We have studied individual indium phosphide (InP) nanowires grown on top of a (111) InP substrate using the vapor-liquid-solid technique in a metal-organic vapor-phase epitaxy (MOVPE) reactor.[24] Arrays of separated nanowires were grown by defining the positions of the gold catalyst particle using electron beam lithography. To ensure that the emission from single nanowires is not affected by their neighbors, the distance between the gold catalyst particles was set to 10 μm. The substrate with the gold particles on top was annealed at temperature $T = 660^{\circ}C$ for 10 minutes prior to the growth to remove the native oxide layer and the remaining organic materials from the surface of the sample. Nanowires were grown at $T = 500^{\circ}C$ for 25 minutes under trimethylindium ($TMIn$) and phosphine (PH_3) flow. To ensure that the diameter of the grown nanowires is uniform along their height, a small additional flow of hydrogen chloride (HCl) was introduced together with $TMIn$ and PH_3. The HCl provided an in-situ etching of the nanowire material preventing it from forming any significant tapering.[25] As can be appreciated in the scanning electron microscopy (SEM) image shown in Figure 1(a), the nanowires have a top diameter of about $d = 100$ nm and a length of $l = 3.13$ μm. InP nanowires grow preferentially in wurtzite structure on top of the zincblende InP substrate.[26] Since the electronic bandgap of InP

in the wurtzite phase is larger by around 50 meV than that of zincblende, the emission peak of wurtzite nanowires is blue-shifted compared to that of the substrate.[27]

A $\lambda = 785$ nm diode laser was used to excite the photoluminescence of nanowires and the substrate. The laser beam was focused to a diffraction limited spot with a $\times 100$, $NA = 0.95$ objective. The photoluminescence was collected by the same objective and sent into a fiber coupled spectrometer. For the details of the experimental configuration see Figure S1 - in supporting information. Figure 1(b) shows the emission spectra of a nanowire and the substrate. The emission of the substrate is centered at $\lambda = 920$ nm, while the emission from the nanowires has a peak at $\lambda = 850$ nm. For the Fourier measurements described next, we used bandpass filters with a center wavelength of $\lambda = 850$ nm and $\lambda = 920$ nm and a bandwidth of 10 nm to separate the emission from the nanowires from the emission from the substrate.

Fourier microscopy. We have resolved the directional emission of individual nanowires using Fourier microscopy. This technique is based on the Fourier transform properties of lenses to obtain the emission pattern of an object in the reciprocal space. A wave collected by an objective lens can be decomposed into individual plane waves, each focusing at a unique position on the back focal plane of the objective (see Figure S2 - supporting information). This plane is imaged by a lens (Fourier lens) onto a CCD camera (Fourier camera), where the image of the reciprocal space of the emission is recorded. By using the appropriate filter in front of the Fourier camera we have obtained images of the emission at the wavelength of interest. The Fourier images are plotted in polar coordinates, where the radius represents the angle of emission θ, and the azimuthal angle φ corresponds to the azimuthal angle of the emission (see inset of Figure 2). We have also analyzed the polarization of the directional emission using a linear polarizer placed on the light path just before the Fourier camera. Along the transmission axis of the polarizer only the p-polarized emission is recorded, while along the direction perpendicular to this transmission axis we detect the s-polarized emission. A detailed explanation of the polarization analysis is given in Figure S3

- supporting information.

The large numerical aperture of the microscope objective ($NA = 0.95$) allows collecting large angles of emission limited by a marginal ray at $\theta_{max} = 72^\circ$ from the normal to the sample. Figure 2(a) shows the Fourier images, in units of counts per second, of the unpolarized emission from a nanowire at $\lambda = 850$ nm. The Fourier images are accompanied by line plots above and on the right, that represent the profiles of the directional emission along the $\varphi = 0^\circ$ and 180° and $\varphi = 90^\circ$ and 270° directions, respectively. The measurement reveals a strong directional feature, namely, a circular emission pattern with a peak at $\theta = 49^\circ$ for all the azimuthal angles φ. Figure 2b displays the polarized directional emission pattern. The transmission axis of the polarizer is indicated in the figure by a white double arrow. The dominant contribution to the directional emission intensity is along the transmission axis of the polarizer, revealing that this emission is p-polarized (see Figure S3 in the supporting information for additional information on the polarization).

The direction and polarization of the emission from nanowires is pronouncedly different from that of Lambertian emitters. To illustrate this difference, we have measured the emission from the flat InP surface by exciting it locally with the focused diode laser. We have collected the emission with the same objective and used a $\lambda = 920$ nm band pass filter to isolate this emission in the Fourier camera. As shown in Figure 3a, the emission pattern from the InP surface shows no particular directional features. This is expected for Lambertian sources where the emitted light is distributed equally in all directions. Also, the emission is not preferentially polarized as displayed in Figures 3(b) and (c). The pronounced difference between the emission of a flat surface and the emission of a nanowire, together with the directional emission of the latter, justifies the term of semiconductor nanoantennas when referring to nanowires.

Numerical simulations. In order to gain physical insight into the emission process from semiconductor nanowires, we have carried out a theoretical analysis including numerical calculations.

First, we aim at reproducing the emission characteristics as close as possible to the experimental results with the help of finite element method (FEM) numerical calculations. A cylindrical InP nanowire of diameter $d = 100$ nm and length $l = 3.13$ μm standing on top of a flat InP substrate is considered. To simulate the nanowire photoluminescence, we place three point electric dipoles with orthogonal dipole moments at the center of the nanowire and radiating at $\lambda = 850$ nm. The Fourier images are calculated by projecting the far field power emitted within a polar angle of 72° with respect to the z axis (nanowire axis) on a plane, as depicted in Figure 4(a). The calculated Fourier images represent the radiated power per unit solid angle, $\frac{dP}{d\Omega}$, normalized by the total power P_{total} emitted by a dipole in a homogeneous InP environment. The simulated Fourier image shows a ring pattern that closely reproduces the experimental result (Figure 2(a)). For comparison we have also calculated the emission pattern of three point electric dipoles with orthogonal orientations at a height of 1.565 μm above the substrate, i.e., without the nanowire. This calculation is displayed in Figure 4(b). We observe an entirely different pattern consisting of a wide, structureless central lobe.

We study the origin of such distinct behavior through a detailed analysis of the polarization of the emission. Figure 5 displays the simulations of the emission patterns for each dipole orientation. Figures 5(a) and (b) represent the unpolarized and polarized emissions, respectively, of the dipole oriented parallel to the nanowire axis, while (c) and (d) are the emission of the dipole oriented perpendicular to this axis. We observe that the ring-like emission pattern is characteristic of the emission from a dipole moment parallel to the nanowire axis, yielding indeed the largest contribution to the total Fourier image. Although weaker, the contributions from the two other dipole moments perpendicular to the nanowire axis, with the emission pattern of a single elongated lobe along the nanowire axis, are also present. This is evidenced by the plots of the cross cuts through the images in Figures 2(a) and 4(a), in which it can be appreciated a significant emission at the center of the Fourier image, that otherwise would be zero.

The excellent agreement between the simulations and the measurements sheds much light onto various aspects of the emission process. Since all dipole orientations contribute to the emission with the same relative weight, photoluminescence excitation in this configuration leads to essentially unpolarized emission.[28] The exact location of the emission within the nanowire is not crucial to the directionality of the emission with the present illumination/excitation conditions, i.e, uniform along the nanowire. To confirm this point, in the simulations we have varied the position of the dipoles along the nanowire axis, leading to very similar results unless emitting from the end facets of the nanowire. Incidentally, by spatially averaging the dipole emission, such edge contributions to the Fourier images would be irrelevant. Despite the inferred uniform excitation and fairly uniform spatial photoluminescence from the whole nanowire, the emission is strongly directional with a preferred polarization. This is fully supported by our numerical calculations, which reveal that the emission of the three orthogonal dipoles are governed by the environment, namely, the nanowire, through its local density of electromagnetic states (LDOS). The nanowire plays thus the role of a nanoantenna, controlling the emission of the dipole by its geometry and dimensions.

To study the antenna properties of the emission in more detail, we have investigated the modes associated to an infinitely long cylinder of identical diameter $d = 100$ nm, as described by the corresponding dispersion relation (see supporting information).[29] At $\lambda = 850$ nm ($\omega d/c = 0.74$), our results in Figure 6(a) show that a leaky mode is excited with a real component of the propagation constant $Re(k_z)d = 0.65$. From $Im(k_z)$, a decay length of 0.715 μm is inferred. At this wavelength and for this nanowire diameter, no coupling occurs to guided modes able to propagate along the nanowire, i.e., modes with $Re(k_z)$ such that $\omega/c < Re(k_z) < n_{InP}\omega/c$, where $n_{InP} = 3.42$ is the real part of the refractive index of InP at $\lambda = 850$ nm. Although the hybrid fundamental guided mode HE_{11} (having no cut-off frequency) is present, its propagation constant coincides with the light line within the spectral range of Figure 6(a). This means that no significant coupling into this weakly guided mode occurs due to fact that its electromagnetic field is mainly localized into the surrounding medium.[30] The leaky mode exhibits the lowest-order symmetry in the predomi-

nant (axial) component of the electric field. As shown in Figure 6(b), the intensity of this mode is maximum at the center of the cylinder and decays radially. The magnetic field correspondingly rotates around the nanowire axis, as shown in Figure 6(d), with a larger intensity near the surface of the cylinder. As a matter of fact, such electromagnetic field pattern of the leaky mode is qualitatively indistinguishable from that obtained for a finite nanowire from full numerical simulations (as in Figure 5). Nevertheless, the fact that such a leaky mode is excited contributes through an enhanced LDOS to an increase in photoluminescence. The excited leaky mode can be associated to a Mie resonance that appears when a plane wave of $\lambda = 850$ nm is incident onto an infinitely long cylinder of an identical diameter, with a polarization along the axis of this cylinder, as revealed by the extinction efficiency shown in Figure 6(a).[13] The electric and magnetic field intensity of such Mie resonance is plotted in Figures 6(c) and (e), respectively, bearing a strong resemblance to the leaky mode symmetry. With regard to the emission directionality, the experimental and numerical results manifest also the influence of the leaky mode excitation, since the typical ring patterns in the emission are a consequence of the nanowire playing the role of a nanoantenna, as commented above.

At this point it is interesting to compare the emission from a source embedded in the nanowire at a height of 1.565 μm with the emission intensity of a dipole in free space at a height of 1.565 μm above the substrate. Figures 7(a) and (b) show the unpolarized, normalized emitted power as a function of the angle of emission for dipoles oriented parallel and perpendicular to the axis of the nanowire, respectively. The angular dependent emitted power is normalized by the total emitted power. The black-solid curves represent the emission of a dipole embedded in the nanowire, while the red-dashed curves illustrate the emission of a dipole above the substrate without the nanowire. As can be appreciated in Figure 7(a), due to the coupling to the leaky mode, the emission of a vertical dipole in the nanowire of diameter $d = 100$ nm is enhanced nearly 4 times with respect to that of a dipole in free space with the same orientation. This is in agreement with the leaky mode symmetry, where the maximum of the electric field parallel to the nanowire axis is located at the center

of the cross section of the nanowire. The fact that such a leaky mode is excited contributes through an enhanced local density of optical states (LDOS) to an increased photoluminescence (recall that the LDOS of the nanowire supporting a single mode is basically governed by the mode local electromagnetic field). At the same time, the symmetry of the leaky mode efficiently suppresses the emission of a dipole perpendicular to the axis of the nanowire, as displayed in Figure 7(b). The efficiency of the emission can be tailored by modifying the diameter of the nanowire. To illustrate that, we have calculated the emission pattern of a nanowire with a diameter of 50 nm, for which light coupling to the TM_0 leaky mode supported at $\lambda = 850$ nm, is less efficient than for 100 nm-thick nanowire. As mentioned above, the (no cut-off) weakly guided mode HE_{11} is also present, but no appreciable coupling of the emission into it takes place.[30] The blue-dotted curves in Figures 7(a) and (b) illustrate the emission from a dipole parallel and perpendicular to the axis of the nanowire, respectively. While the thin nanowire can still enhance the emission of a parallel dipole with respect to a dipole in free space, this enhancement is significantly lower than for the $d = 100$ nm nanowire. The emission of a perpendicular dipole is further suppressed. We note that for thicker wires than those investigated here, it is possible to efficiently couple the emission to guided modes in the cylindrical structure. These guided modes lead to an even more pronounced directional emission that can be controlled by varying the nanowire diameter and length. This rich interplay of various geometrical parameters in the nanowire antenna emission will be described in a future publication. The directional emission of nanowires is important for the design and optimization of nanowire-based light emitting diodes and single photon sources. The design of efficient light sources needs to consider the dimensions of the nanowires that determine the solid angle of the emission. By reciprocity, it is expected that the optical absorption efficiency of semiconductor nanowires strongly depends on the angle of incidence of light. Therefore, the antenna-like behavior of nanowires will have an impact on the design of nanowire-based solar cells.

In conclusion, by measuring the directional and polarized emission of single nanowires using Fourier microscopy, we have demonstrated the antenna-like emission of these nanostructures.

Finite element simulations of a dipole source embedded in a nanowire provided an excellent agreement with the measurements. Similar to RF linear antennas, semiconductor nanowires exhibit a directional and an enhanced emission due to resonances in the structure. The directional emission is ruled by the leaky modes supported by nanowires. These modes are also responsible for a modification of the local density of optical states and for the enhancement of the emission of dipoles with a certain dipole moment relative to the nanowire orientation and the inhibition of the emission for other orientations. This demonstration of nanoantenna emission from semiconductor nanowires is of relevance for designing the novel nanowire light emitting diodes and single photon sources with tailored emission characteristics.

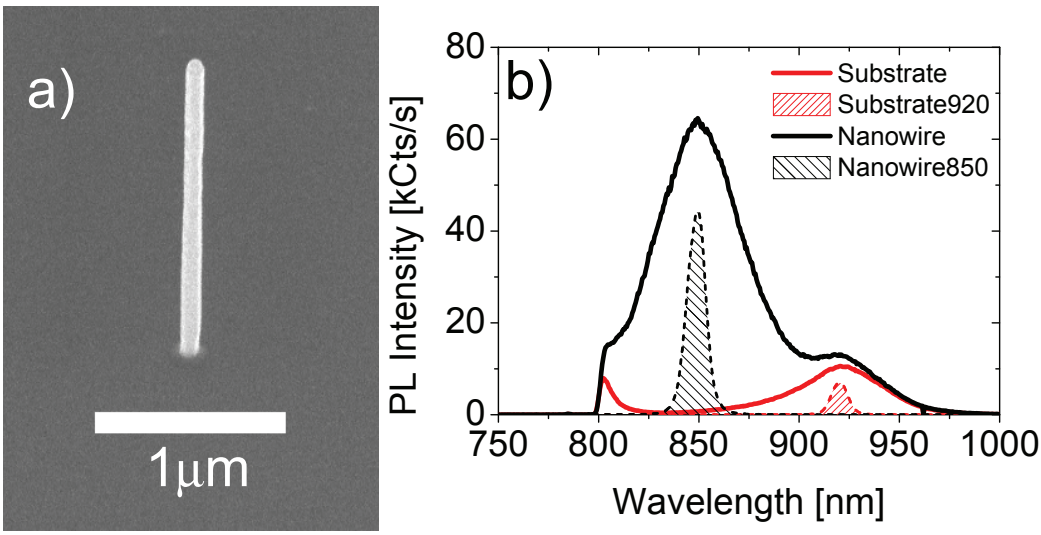

Figure 1: a) Scanning Electron Microscope image taken at an inclination of 30° of an InP nanowire grown on top of an InP substrate . The nanowire is 3.13 μm long and has a diameter of 100 nm. b) Photoluminescence spectra of the nanowire (black line) and the substrate (red line), where a long-pass filter with a cut-off wavelength of 800 nm is used to filter out the scattered light from the pump laser ($\lambda = 785$ nm). The photoluminescence transmitted through a band pass filter with a central wavelength of $\lambda = 850$ nm (10 nm at FWHM) and $\lambda = 920$ nm (10 nm at FWHM) are represented by the black and red dashed lines, respectively.

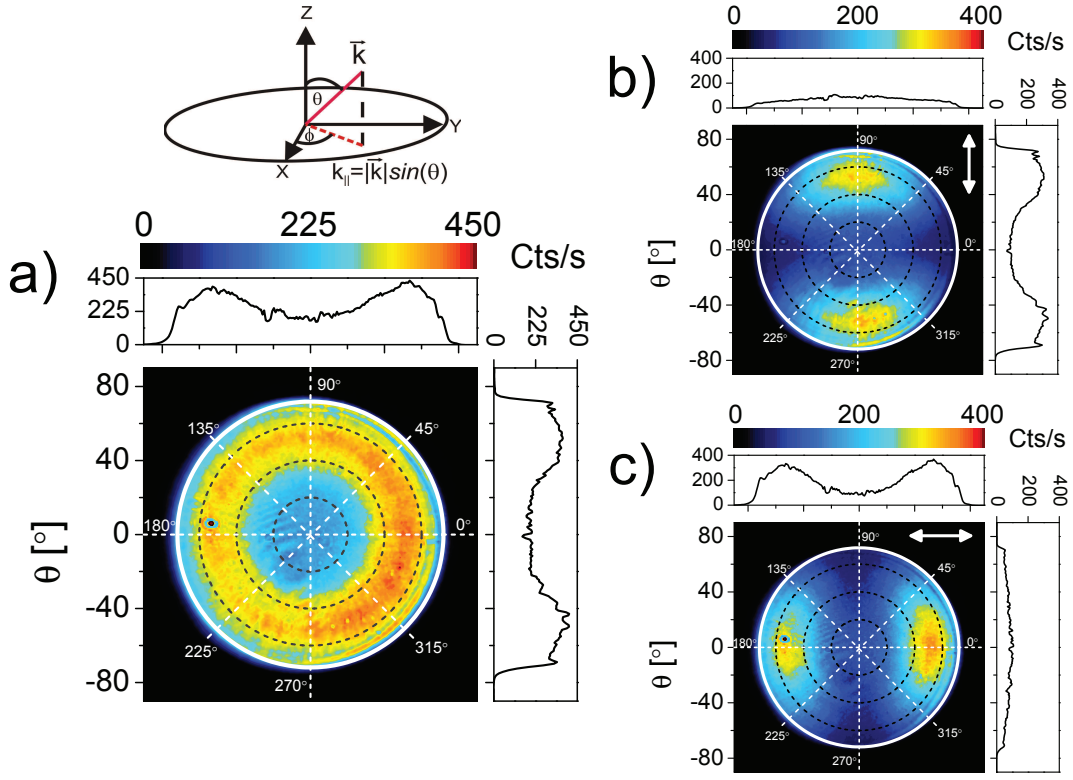

Figure 2: Fourier images of the emission from InP nanowires at $\lambda = 850$ nm taken using a bandpass filter with a central wavelength of $\lambda = 850$ nm (bandwidth of 10 nm at FWHM). a) Fourier image of the unpolarized emission, b) Fourier image taken with a polarizer with the transmission axis along the vertical direction ($\varphi = 90°$ and 270°). c) Fourier image taken with a polarizer with the transmission axis along the horizontal direction ($\varphi = 0°$ and 180°). The alignment of the transmission axis of the polarizer is indicated by the white double arrow in (b) and (c). The graphs on the top and right side of each figure show the profiles of the Fourier images along the horizontal and vertical directions crossing at the center of the images.

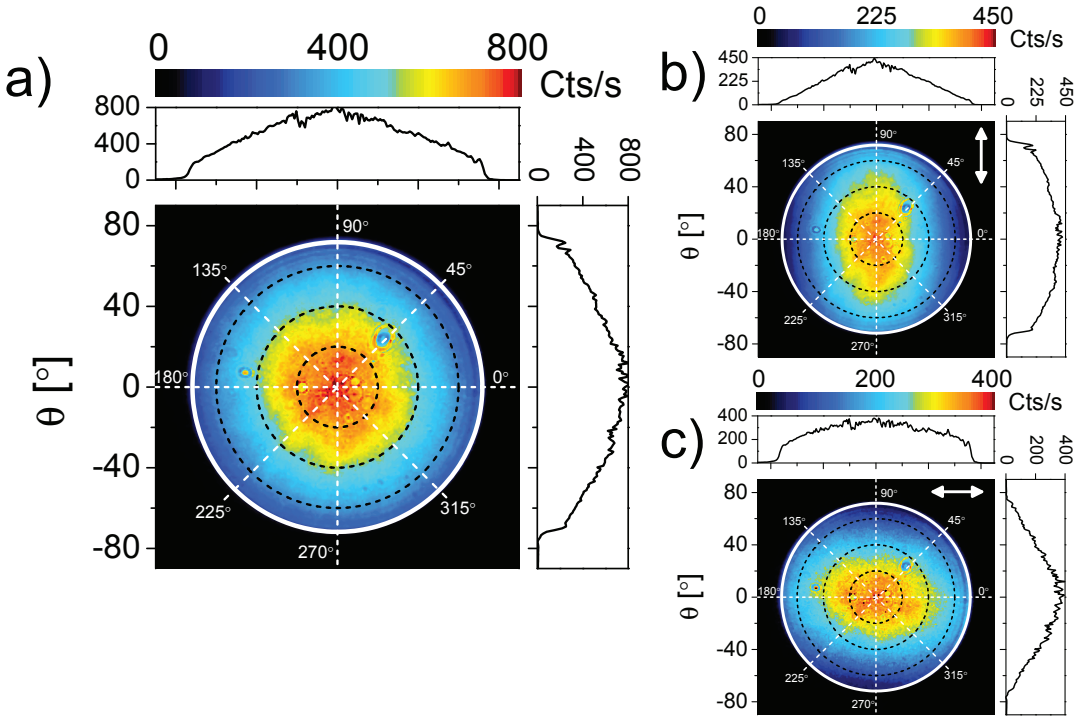

Figure 3: a) Fourier image of the unpolarized photoluminescence of an InP substrate at $\lambda = 920$ nm taken using a bandpass filter with a central wavelength of $\lambda = 920$ nm (bandwidth of 10 nm at FWHM). b) Directional emission from InP substrate taken using a polarizer with the transmission axis in the vertical direction ($\varphi = 90°$ and $270°$). c) Directional emission from InP substrate taken using a polarizer with the transmission axis aligned along the horizontal direction ($\varphi = 0°$ and $180°$). The direction of the transmission axis of the polarizer is depicted by the white double arrow. The graphs on the top and right side of the figure show the profiles of the Fourier images along the horizontal and vertical directions crossing at the center of the images.

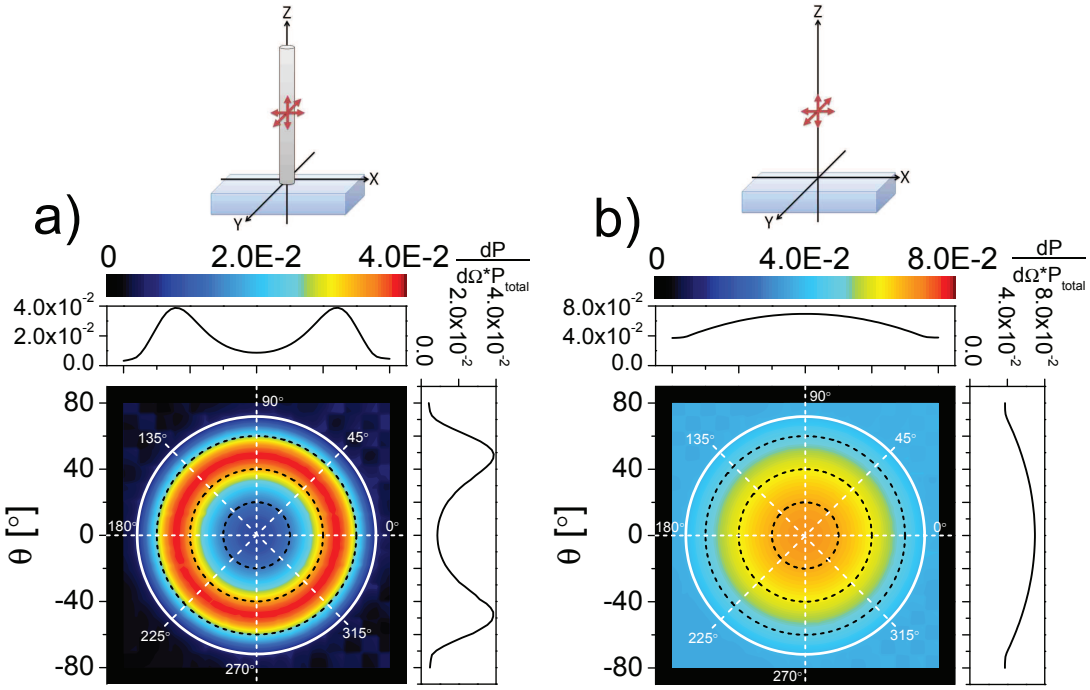

Figure 4: a) FEM simulations of the unpolarized directional emission from 3 orthogonal dipoles located in the middle of the 3.13 µm nanowire standing on top of an InP substrate. The dipoles radiate at a wavelength of $\lambda = 850$ nm. b) Simulations of the directional emission from 3 orthogonal dipoles placed 1.565 µm above the InP substrate without the presence of a nanowire. On the top are schematic representations of the simulated configurations.

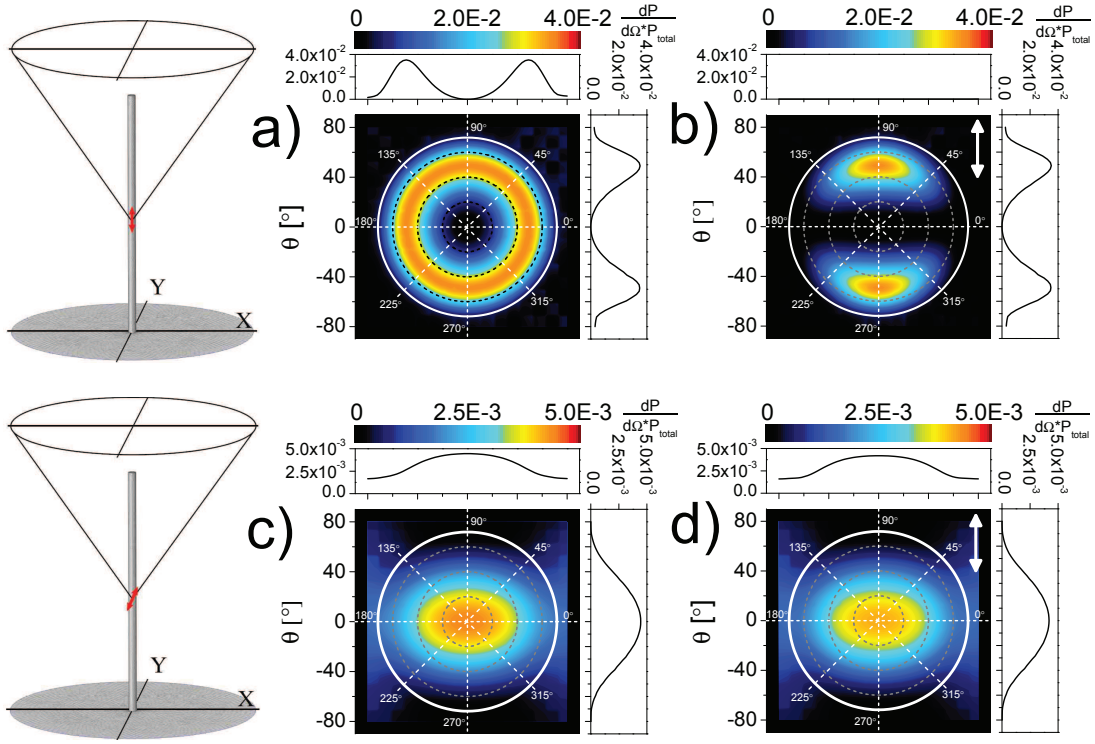

Figure 5: Simulations of the directional emission from a dipole located in the middle of the nanowire standing on top of an InP substrate. The dipole radiates at a wavelength of $\lambda = 850$ nm. On the left: schematics of the simulated configuration: an InP nanowire with a diameter of $d = 100$ nm and length of $l = 3.13$ µm containg a dipole with a dipole moment parallel to the long axis of the nanowire (top) and perpendicular (bottom). a) Unpolarized directional emission pattern from the dipole oriented parallel to the axis of the nanowire. b) Polarized directional emission of the dipole parallel to the axis of the nanowire with a polarization along the vertical direction on the image ($\varphi = 90°$ and $270°$, indicated by the white double arrow). c) Unpolarized directional emission pattern from the dipole oriented perpendicular to the long axis of the nanowire. d) Polarized directional emission of the dipole perpendicular to the axis of the nanowire with a polarization along the vertical direction on the image ($\varphi = 90°$ and $270°$, indicated by the white double arrow).

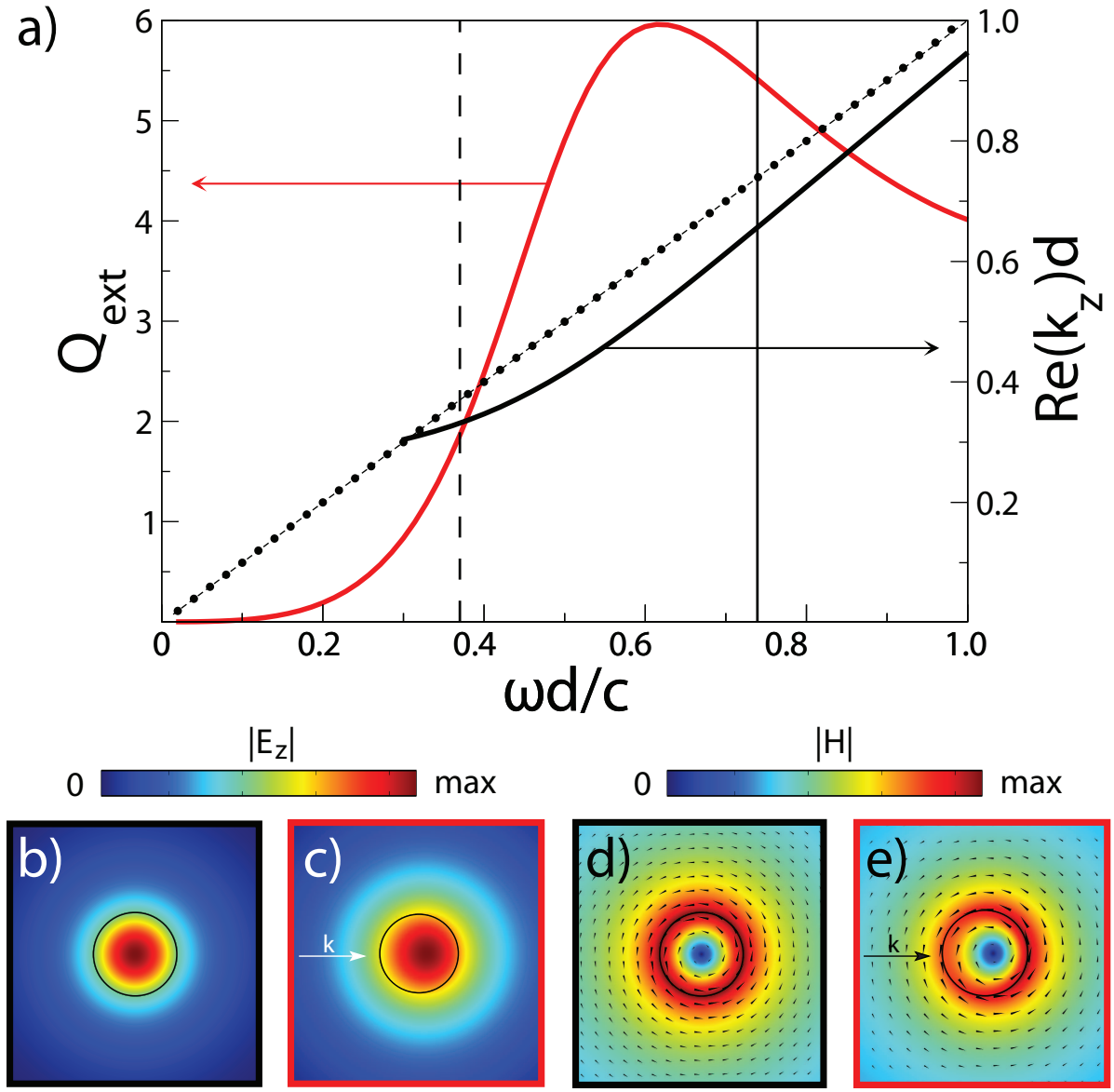

Figure 6: a) Dispersion relations of the leaky mode (black curve) and the weakly guided HE_{11} mode (black dots) supported by an infinite InP cylinder (fixed wavelength at 850 nm, $n_{InP} = 3.42$, with varying diameter d). The short-dashed line nearly on top of the HE_{11} mode represents the light line. Dispersion relations refer to the right axis in the plot. Mie extinction efficiency (red curve, corresponding to the left axis in the plot) of the same InP nanowire when a p-polarized plane wave impinges perpendicular to the cylinder axis. The vertical solid line indicates the particular case $d = 100$ nm and the vertical long-dashed line indicates $d = 50$ nm. b) Contour map of the magnitude of the z-component of the electric field of the leaky mode. c) Contour map of the magnitude of the z-component of the electric field scattered by the same cylinder in Mie resonance. The white arrow indicates the incident wave vector. c) Contour map of the in-plane magnetic field magnitude of the leaky mode. d) Contour map of the in-plane magnetic field magnitude scattered by the same cylinder in Mie resonance. The long black arrow indicates the incident wave vector. The small black arrows in c) and d) indicate the directions of the in-plane magnetic field vector.

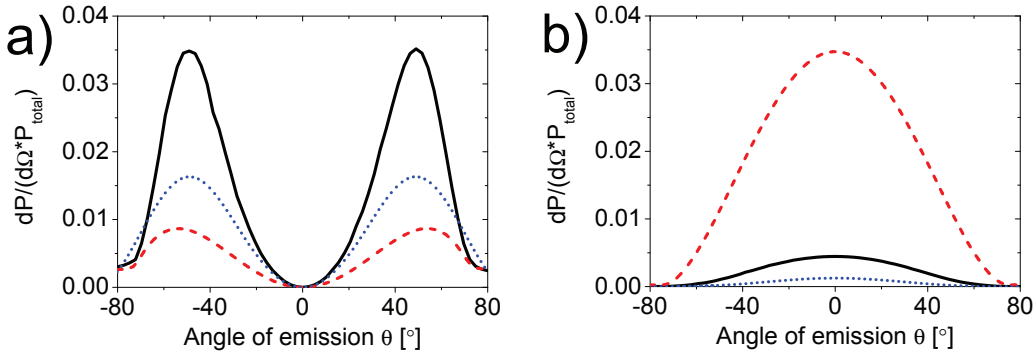

Figure 7: Emitted power as a function of the emission angle emission, normalized by the total emitted power P_{total}, calculated for a) a dipole oriented parallel to the axis of the nanowire, and b) a dipole with perpendicular orientation with respect to the axis of the nanowire. The calculations are made for two nanowire diameters, $d = 100$ nm (black-solid curves) and $d = 50$ nm (blue-dotted curves), both with a length of 3.13 μm. The red-dashed curves correspond to a calculation of the emitted power of a dipole in free space at a height of above the 1.565 μm substrate.

Acknowledgement

The authors are grateful to Tilman Zehender and Erik P. A. M. Bakkers for providing the sample used in the experiments. This work is part of the research program of the "Stichting voor Fundamenteel Onderzoek der Materie (FOM)", which is financially supported by the "Nederlandse organisatie voor Wetenschappelijk Onderzoek (NWO)" and is part of an industrial partnership program between Philips and FOM. The work of Ramón Paniagua-Domínguez and José A. Sánchez-Gil has been supported in part by the Spanish "Ministerio de Economía y Competitividad" (projects consolider-Ingenio EMET CSD2008-00066 and NANOPLAS FIS2009-11264) and the "Comunidad de Madrid" (MICROSERES network S-2009/TIC1476). Ramón Paniagua-Domínguez acknowledges support from CSIC through a JAE-Pre grant.

Supporting Information Available

Supporting information shows the schematics of the experimental setup, Fourier transform properties of lenses, polarization analysis in the setup, principles of wave propagation in cylindrical geometry and the description of the numerical methods.

This material is available free of charge via the Internet at `http://pubs.acs.org/`.

References

(1) Bakkers, E. P. A. M.; van Dam, J. A.; De Franceschi, S.; Kouwenhoven, L. P.; Kaiser, M.; Verheijen, M.; Wondergem, H.; van der Sluis, P. *Nat. Mater.* **2004**, *3*, 769–773.

(2) Mårtensson, T.; Svensson, C. P. T.; Wacaser, B. A.; Larsson, M. W.; Seifert, W.; Deppert, K.; Gustafsson, A.; Wallenberg, L. R.; Samuelson, L. *Nano letters* **2004**, *4*, 1987–1990.

(3) Gudiksen, M.; Lauhon, L.; Wang, J.; Smith, D.; Lieber, C. M. *Nature* **2002**, *415*, 617–620.

(4) Lauhon, L. J.; Gudiksen, M. S.; Wang, D.; Lieber, C. M. *Nature* **2002**, *420*, 57–61.

(5) Huang, M. H.; Mao, S.; Feick, H.; Yan, H.; Wu, Y.; Kind, H.; Weber, E.; Russo, R.; Yang, P. *Science* **2001**, *292*, 1897.

(6) Johnson, J. C.; Yan, H.; Schaller, R. D.; Haber, L. H.; Saykally, R. J.; Yang, P. *J. Phys. Chem. B* **2001**, *105*, 11387–11390.

(7) Scofield, A. C.; Kim, S.-H.; Shapiro, J. N.; Lin, A.; Liang, B.; Scherer, A.; Huffaker, D. L. *Nano Lett.* **2011**, *11*, 5387–5390.

(8) Panev, N.; Persson, A.; Sköld, N.; Samuelson, L. *Appl. Phys. Lett.* **2003**, *83*, 2238.

(9) van Weert, M. H. M.; Akopian, N.; Kelkensberg, F.; Perinetti, U.; van Kouwen, M. P.; Gómez Rivas, J.; Borgström, M. T.; Algra, R. E.; Verheijen, M. A.; Bakkers, E. P. A. M. *small* **2009**, *5*, 2134–2138.

(10) Claudon, J.; Bleuse, J.; Malik, N. S.; Bazin, M.; Jaffrennou, P.; Gregersen, N.; Sauvan, C.; Lalanne, P.; Gérard, J. M. *Nat. Photonics* **2010**, *4*, 174–177.

(11) Wang, J.; Gudiksen, M. S.; Duan, X.; Cui, Y.; Lieber, C. M. *Science* **2001**, *293*, 1455.

(12) Seo, K.; Wober, M.; Steinvurzel, P.; Schonbrun, E.; Dan, Y.; Ellenbogen, T.; Crozier, K. B. *Nano Lett.* **2011**, *11*, 1851–1856.

(13) Bohren, C. F.; Huffman, D. R. *Absorption and scattering of light by small particles*; Wiley, New York, 1983.

(14) Ruda, H. E.; Shik, A. *J. Appl. Phys.* **2006**, *100*, 024314–024314.

(15) Cao, L.; White, J. S.; Park, J. S.; Schuller, J. A.; Clemens, B. M.; Brongersma, M. L. *Nat. Mater.* **2009**, *8*, 643–647.

(16) Brönstrup, G.; Jahr, N.; Leiterer, C.; Csáki, A.; Fritzsche, W.; Christiansen, S. *ACS Nano* **2010**, *4*, 7113–7122.

(17) Johnson, J. C.; Yan, H.; Yang, P.; Saykally, R. J. *J. Phys. Chem. B* **2003**, *107*, 8816–8828.

(18) van Vugt, L. K.; Rühle, S.; Vanmaekelbergh, D. *Nano Lett.* **2006**, *6*, 2707–2711.

(19) Babinec, T. M.; Hausmann, B. J. M.; Khan, M.; Zhang, Y.; Maze, J. R.; Hemmer, P. R.; Lončar, M. *Nat. Nanotech.* **2010**, *5*, 195–199.

(20) Maslov, A. V.; Ning, C. Z. *Opt. Lett.* **2004**, *29*, 572–574.

(21) Maslov, A. V.; Bakunov, M. I.; Ning, C. Z. *J. Appl. Phys.* **2006**, *99*, 024314–024314.

(22) Bharadwaj, P.; Deutsch, B.; Novotny, L. *Adv. Opt. Photon.* **2009**, *1*, 438–483.

(23) Giannini, V.; Fernández-Domínguez, A. I.; Heck, S. C.; Maier, S. A. *Chem. Rev.* **2011**, *111*, 3888–3912.

(24) Wagner, R. S.; Ellis, W. C. *Appl. Phys. Lett.* **1964**, *4*, 89–90.

(25) Borgström, M.; Wallentin, J.; Trägårdh, J.; Ramvall, P.; Ek, M.; Wallenberg, L.; Samuelson, L.; Deppert, K. *Nano Research* **2010**, *3*, 264–270.

(26) Glas, F.; Harmand, J. C.; Patriarche, G. *Phys. Rev. Lett.* **2007**, *99*, 146101.

(27) Mattila, M.; Hakkarainen, T.; Mulot, M.; Lipsanen, H. *Nanotechnology* **2006**, *17*, 1580.

(28) Kira, M.; Jahnke, F.; Koch, S. W. *Phys. Rev. Lett.* **1998**, *81*, 3263–3266.

(29) Stratton, J. A. *Electromagnetic Theory. International Series in Pure and Applied Physics*; McGraw-Hill Book Company, New York, 1941.

(30) Ramo, S.; Whinnery, J.; Van Duzer, T. *Fields and waves in communication electronics*; Wiley, New York, 1993.

Graphical TOC Entry

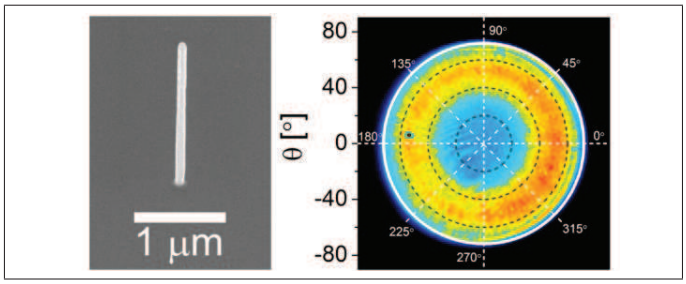

Supporting information for:

Nanowire antenna emission

Grzegorz Grzela,[*,†] Ramón Paniagua-Domínguez,[‡] Tommy Barten,[†] Yannik Fontana,[†,§] José A. Sánchez-Gil,[‡] and Jaime Gómez Rivas[†,¶]

FOM Institute for Atomic and Molecular Physics (AMOLF), c/o Philips Research, High-Tech Campus 4, 5656 AE Eindhoven, The Netherlands, Instituto de Estructura de la Materia (IEM-CSIC), Consejo Superior de Investigaciones Científicas, Serrano 121, E-28006 Madrid, Spain, and COBRA Research Institute, Eindhoven University of Technology, P.O. Box 513, 5600 MB Eindhoven, The Netherlands

E-mail: grzela@amolf.nl

Experimental setup. The schematics of the Fourier microscope used in this work is presented in Figure S1. We excite the photoluminescence in individual InP nanowires using a $\lambda = 785$ nm diode laser with an initial power of 40 mW. The laser beam is expanded and coupled to a microscope objective by using a beam splitter. The expanded beam covers the full back aperture of the objective, which allows focusing the beam into a diffraction limited spot. In the experiments we use a high numerical aperture ($NA = 0.95$) $\times 100$ apochromatic objective. Emission from the nanowire is collected by the same objective and after being transmitted through the beam splitter, it can be directed to a fiber-coupled Czerny-Turner spectrograph with a silicon detector. In this

[*]To whom correspondence should be addressed

[†]FOM Institute for Atomic and Molecular Physics (AMOLF)

[‡]Consejo Superior de Investigaciones Científicas (CSIC)

[¶]Eindhoven University of Technology (TU/e)

[§]Current address: Laboratoire des Matériaux Semiconducteurs, Institut des Matériaux, Ecole Polytechnique Fédérale de Lausanne, 1015 Lausanne, Switzerland

case we filter the pump beam by using a $\lambda = 800$ nm longpass filter. An alternative optical path is used for the directional emission measurements. In this path we use a lens (Fourier lens) to image the back focal plane of the microscope objective on a CCD camera (Fourier camera).

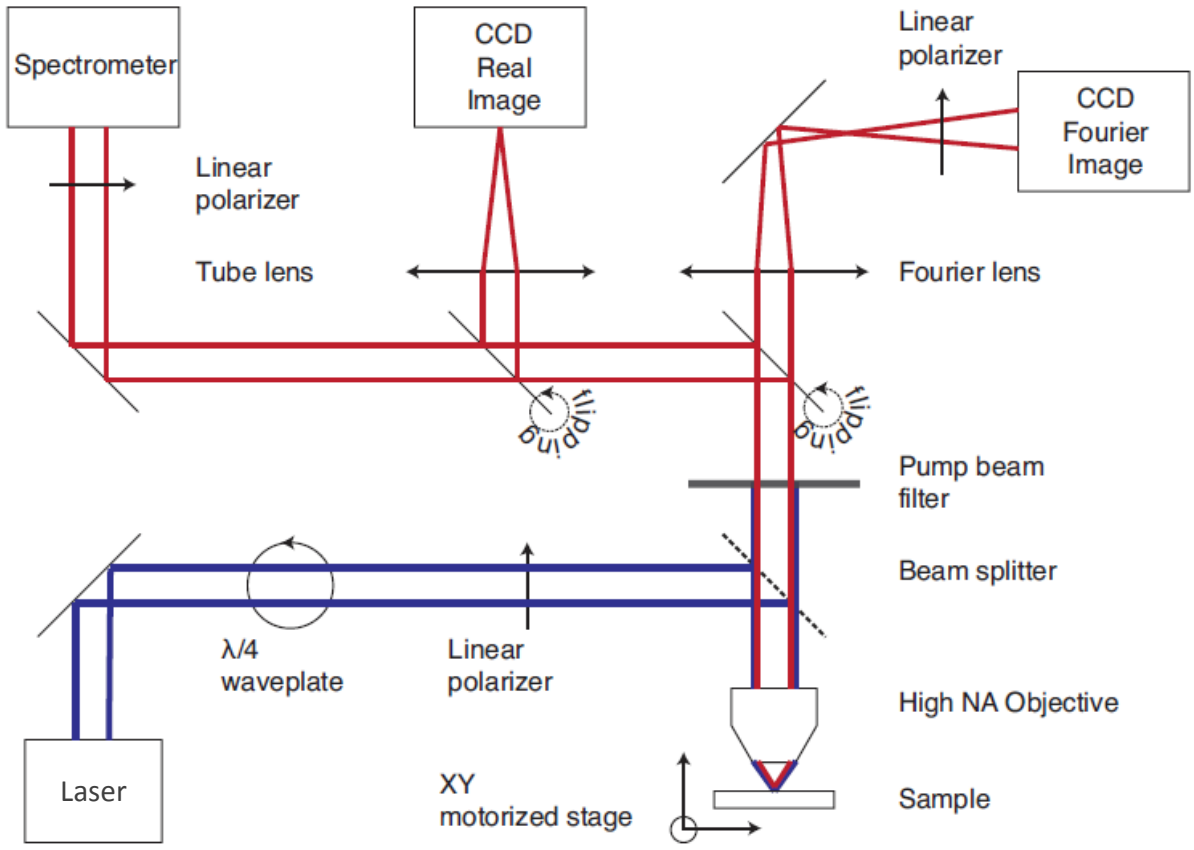

Figure S1: Fourier microscope setup scheme.

The back focal plane of the objective contains the information of the directionality of the emission, as can be appreciated in Figure S2. Radiation emitted from the sample can be described as a superposition of plane waves, each defined by an unique wave wector (in reciprocal space). The objective lens focuses each individual plane wave into a spot with unique spatial coordinates at the back focal plane of the objective. In other words, the electric field distribution at the plane of the lens is Fourier transformed at the back focal plane.[S1]

The Fourier microscope was calibrated by measuring the surface emission from an InP wafer. This emission was also measured by rotating an optical fiber connected to a spectrometer around the sample. Measurements with the rotation stage setup showed a near-Lambertian emission profile of the InP surface for both polarizations.

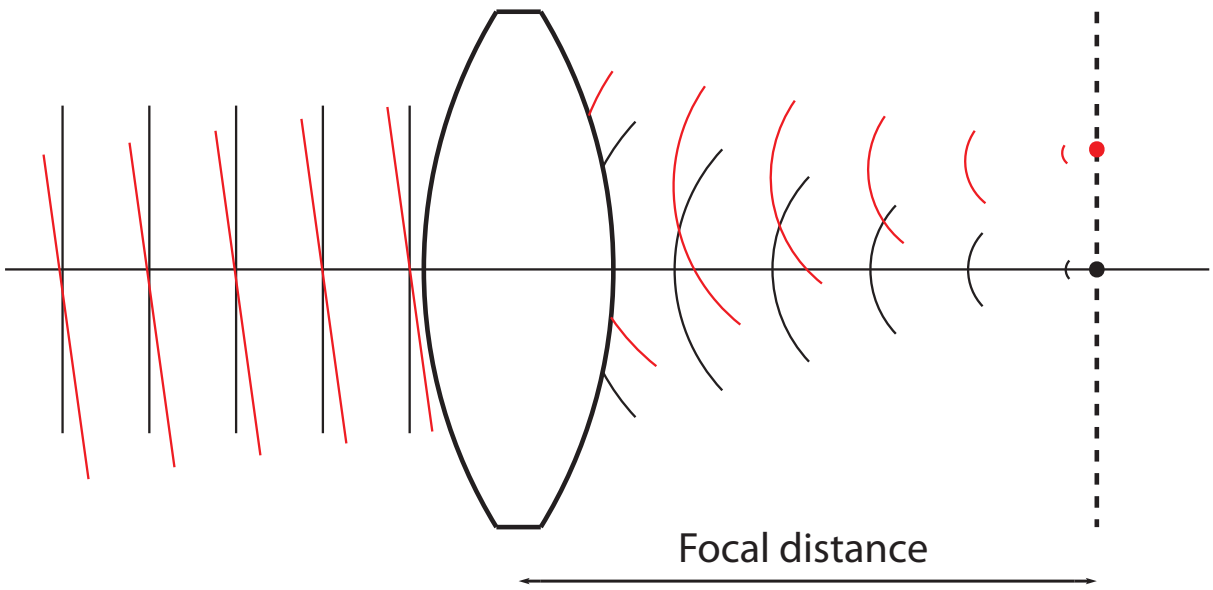

Figure S2: Fourier transform properties of lenses. Two plane waves are incident on a lens from two different directions are focused into two spots, each with unique spatial coordinates on the back focal plane of the lens. The back focal plane is defined as the plane perpendicular to the optical axis of the lens at a focal distance.

Polarization analysis in Fourier microscope. Figure S3 describes the polarization analysis in the Fourier microscope setup. Light emitted from the sample can be p- and s-polarized. The electric field vector of the p-polarized emission (green arrows) lies in the plane containing the wave vector of the emission (single red arrows) and the normal to the sample surface. The s-polarized emission is characterized by the electric field vector perpendicular to that plane (blue arrows). After reaching a microscope objective, the electric field vectors of the emission are projected on the plane perpendicular to the sample surface normal. By using a linear polarizer, the electric field component perpendicular to the transmission axis of the polarizer (double red arrow) is not transmitted. Along the diameter parallel to the transmission axis, the only transmitted light is

p-polarized. Along the diameter perpendicular to the transmission axis of the polarizer only s-polarized emission is transmitted. Along every other azimuthal direction, the transmitted light is a superposition of the s- and p-polarized emission.

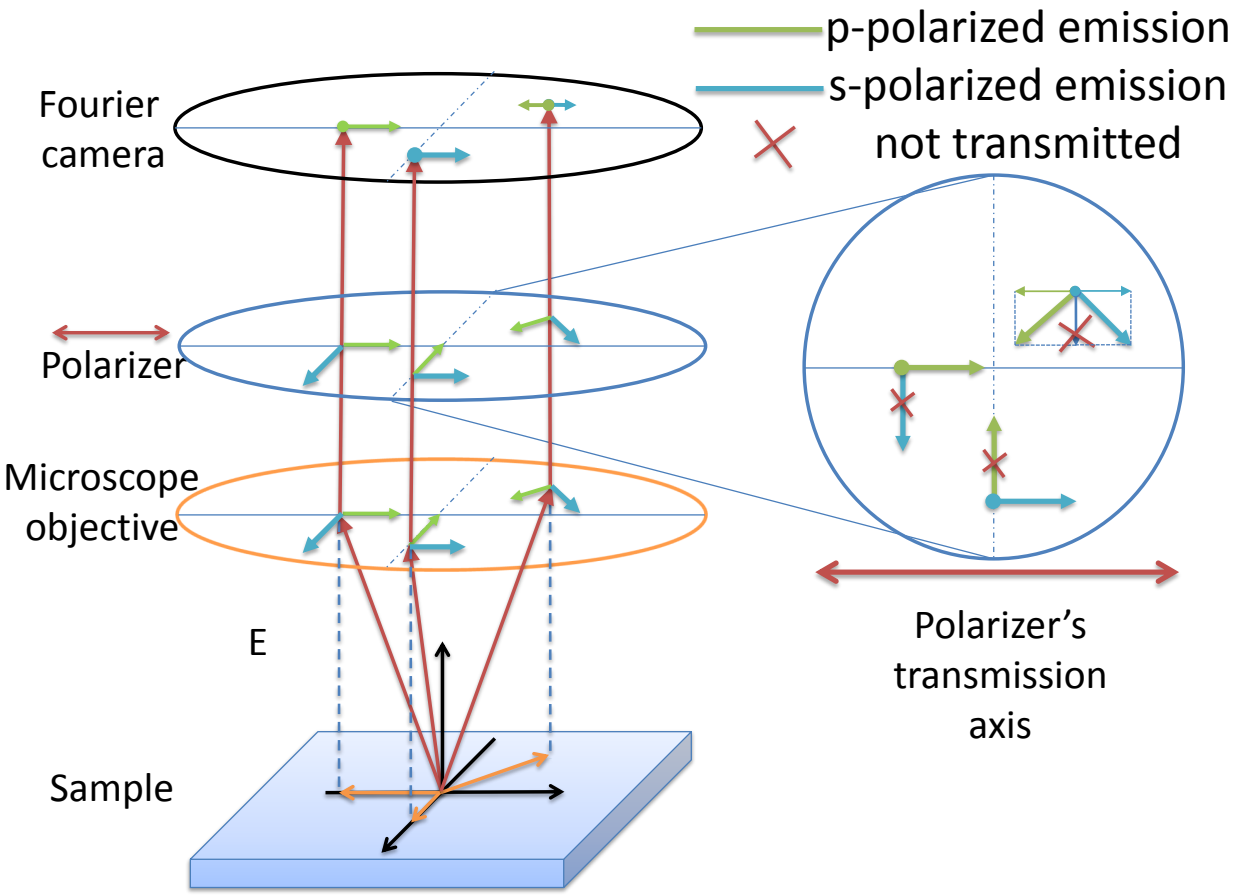

Figure S3: Polarization of the emission in the Fourier microscope.

Electromagnetic wave propagation in an infinite circular cylinder. Assume $n_c = (\varepsilon_c \mu_c)^{1/2}$ and $n = (\varepsilon\mu)^{1/2}$ to be the refractive indices of an infinitely long circular cylinder of radius R and the external medium respectively. No restrictions are imposed to the values of these quantities. The fields in a cylindrical geometry can be expanded in terms of the Bessel (J_m) and Hankel (H_m) functions, which are the elementary wavefunctions of the wave equation in cylindrical coordinates. The electromagnetic boundary conditions are applied for the fields and wave vector at $r = R$ in order to determine the coefficients of the expansion. We obtain a homogeneous system of linear equations for the coefficients that admit non-trivial solutions only when its determinant is not zero.

This condition leads to the characteristic equation that defines the dispersion relation of the modes of the cylinder. The transverse component of the wave vector inside and outside the cylinder are given by

$$k_c^2 = K_c^2 - k_z^2 = n_c^2 \frac{\omega^2}{c^2} - k_z^2, \tag{1}$$

$$k^2 = K^2 - k_z^2 = n^2 \frac{\omega^2}{c^2} - k_z^2, \tag{2}$$

where k_z is continuous at the interface.

Once frequency and material properties are fixed, the values of k_z determine the allowed solutions. The values with a wave vector k purely imaginary, therefore with $k_z^2 > K^2$ (and k_z real if lossless materials are considered), are modes confined to the cylinder (so called guided), since they decay exponentially away from the cylinder. In this case, the value of k_z determines the propagation constant (thus the effective wavelength) of the guided mode. If k_z is not purely real, but has an imaginary component, the fields decay exponentially as they propagate along the cylinder. As they decay, these modes lose energy, which is "leaked" out of the cylinder. The decay length (L_d) is defined as the length at which $I/I_0 = 1/e$, and thus, it is related to Im(k_z) by

$$e^{-2Im(k_z)L_d}. \tag{3}$$

A full description of the problem can be found in, e.g., Stratton's book "Electromagnetic Theory".[S2]

Numerical methods. Finite-element-method-based numerical simulations were performed using commercial software COMSOL Multiphysics v4.2. The simulated space consisted on a circular cylinder of length l and diameter d, representing the nanowire, two concentric spheres of radii $0.7l$ and $0.9l$, respectively, with their centers coinciding with the one of the cylinder and a plane perpendicular to its axis, passing through one of the ends, and splitting the spherical domain and the outer shell into two subdomains. That part of the spherical domain in which the cylinder is located

was set to be air, while the other part, simulating the substrate, and the cylinder were set to be InP, with material constants taken from Palik's book.[S3] Both parts of the outer shell were defined as perfectly matched layers (PML) to absorb all the outgoing radiation, each one with the same index as the adjacent domain to avoid unphysical reflections. The meshing was done with the program built-in algorithm, which creates a tetrahedral mesh. The mesh maximum element size (MES), which limits the maximum size of the edges of the tetrahedrons, was set to be 20 nm in the domain representing the wire, 60 nm in the one representing the substrate, and 80 nm for the elements separating the air and the PML. All the rest of the meshing was set to have a MES of 120 nm. The maximum element growth rate was set to 1.3 in the wire domain, and 1.35 in all remaining domains. Direct PARDISO solver was used to solve the problem.[S4,S5] The package PARDISO is a software for solving large sparse symmetric and unsymmetric linear systems of equations based on fast factorization pivoting methods, that is included within COMSOL Multiphysics. Simulations were highly memory demanding (typically more than 150 GB) and took about one hour per wavelength simulation on a 22 CPUs computing station.

References

(S1) Goodman, J. W. *Introduction to Fourier optics*; McGraw-Hill, New York, 1996; Chapter 5.2.

(S2) Stratton, J. A. *Electromagnetic Theory. International Series in Pure and Applied Physics*; McGraw-Hill Book Company, New York, 1941.

(S3) Palik, E.; Ghosh, G. *Handbook of optical constants of solids*; Academic press, 1998; Vol. 3.

(S4) Schenk, O.; Gärtner, K. *Future Generation Computer Systems* **2004**, *20*, 475–487.

(S5) Schenk, O.; Gärtner, K. *Electronic Transactions on Numerical Analysis* **2006**, *23*, 158–179.

NANO LETTERS

Addition/Correction

pubs.acs.org/NanoLett

Correction to Nanowire Antenna Emission

Grzegorz Grzela,* Ramón Paniagua-Domínguez, Tommy Barten, Yannik Fontana, José A. Sánchez-Gil, and Jaime Gómez Rivas

Nano Lett. **2012**, *12* (11), 5481−5486; DOI: 10.1021/nl301907f

The dispersion relation of the leaky mode shown in Figure 6 of the original manuscript is partially incorrect. Also, the captions to the original Figure 6b−e refer to electric and magnetic field intensities, whereas the field magnitudes are actually plotted. The corrected dispersion relation is included below in Figure 1 with a proper caption indicating the magnitudes of the plotted fields. These corrections affect none of the simulations of the original Letter, since the mode wave vector is not explicitly used in the numerical implementation. Moreover, the mode wave vector for the 100-nm-thick nanowire obtained from the dispersion relation given in Figure 1 has the same value as that given in the original manuscript.

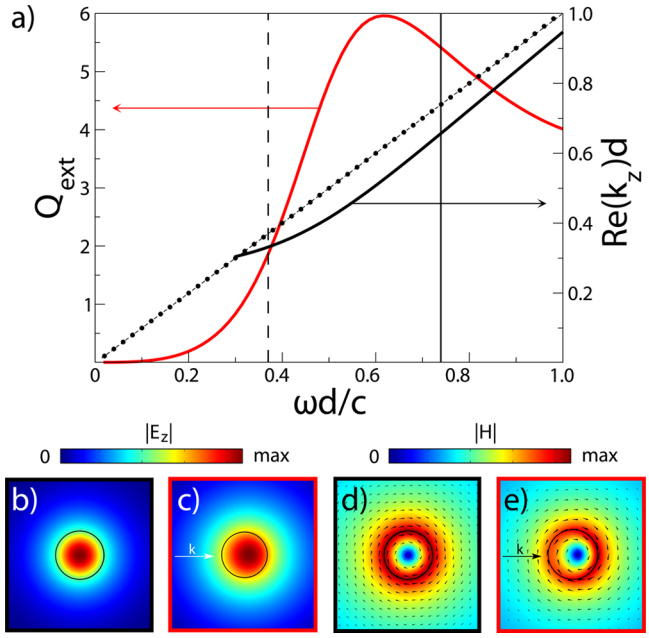

Figure 1. (a) Dispersion relations of the leaky mode (black curve) and the weakly guided HE_{11} mode (black dots) supported by an infinite InP cylinder (fixed wavelength at 850 nm, n_{InP} = 3.42, with varying diameter d). The short-dashed line nearly on top of the HE_{11} mode represents the light line. Dispersion relations refer to the right axis in the plot. The red curve (corresponding to the left axis in the plot) represents the Mie extinction efficiency of the same InP cylinder illuminated with a plane wave with a wave vector perpendicular to the axis of the cylinder and polarized parallel to this axis (p-polarization). The vertical solid line indicates the particular case d = 100, and the vertical long-dashed line indicates d = 50 nm. (b) Contour map of the magnitude of the z-component of the electric field of the leaky mode. (c) Contour map of the magnitude of the z-component of the electric field scattered by the same cylinder in Mie resonance. The white arrow indicates the incident wave vector. (d) Contour map of the in-plane magnetic field magnitude of the leaky mode. (e) Contour map of the in-plane magnetic field magnitude scattered by the same cylinder in Mie resonance. The long black arrow indicates the incident wave vector. The small black arrows in d and e indicate the directions of the in-plane magnetic field vector.

It should be noted that, according to the dispersion relation given in Figure 1, there exists a leaky TM_0 mode for a nanowire with a diameter of 50 nm ($\omega d/c$ = 0.37, marked with a vertical dashed line in Figure 1), contrary to the calculations of Figure 6 of the original manuscript. However, the electric field profile of the TM_0 mode in 50-nm-thick nanowire leads to an inefficient coupling of the dipole radiation to this mode. Moreover, the imaginary component of the wave vector of this leaky mode is about 5 times larger than that of the same mode in a 100-nm-thick nanowire, making the mode very leaky (almost no guidance). Due to such a large imaginary component of the wave vector of this mode, a small fraction of dipole radiation still coupled to the mode produces the radiation pattern that closely resembles that of a free dipole,[1] enhanced or inhibited by its corresponding local density of states. This is indeed corroborated by the simulated directional emission patterns shown in Figure 7a and b of the original manuscript.

REFERENCES

(1) Snyder, A. W.; Love, J. *Optical waveguide theory*; Springer: New York, 1983; Vol. *190*.

Published: November 20, 2013

